BIO-BASED GRAPHENE FROM THE OIL PALM EMPTY FRUIT BUNCHES AS A FLUID LOSS ADDITIVE IN THE WATER-BASED DRILLING MUD

MUHAMMAD TAQI-UDDEEN BIN SAFIAN

UNIVERSITI SAINS MALAYSIA

2024

BIO-BASED GRAPHENE FROM THE OIL PALM EMPTY FRUIT BUNCHES AS A FLUID LOSS ADDITIVE IN THE WATER-BASED DRILLING MUD

by

MUHAMMAD TAQI-UDDEEN BIN SAFIAN

Thesis submitted in fulfilment of the requirements
for the degree of
Doctor of Philosophy

April 2024

ACKNOWLEDGEMENT

First and foremost, I would like to express my heartfelt appreciation and gratitude to Allah SWT, the Almighty, the Most Gracious, upon whom we rely for guidance and sustenance. I extend my deepest thanks to my supervisor, Professor Dr. Mohamad Nasir Mohamad Ibrahim, for his exceptional leadership, invaluable guidance, and unwavering support throughout my journey. I am also grateful to my co-supervisor, Dr. Pandian Bothi Raja, for generously sharing his expertise and providing me with guidance along the way. I am indebted to the Deans of the Institute of Postgraduate Studies and the School of Chemical Sciences at Universiti Sains Malaysia (USM) for granting me the opportunity to pursue my studies and for providing essential research resources. Furthermore, I am grateful to the Malaysian Ministry of Higher Education for their financial support in the form of a research grant (203/PKIMIA/6740073). I extend my sincere appreciation to Mr. Alfred Chee of MPC Cleantech Sdn Bhd for his belief in me and continuous financial support throughout my tenure at USM. I am also thankful to the research groups (Dr. Khalid Umar, Siti Hajar, Najwa Najihah), and the FYP students, Umirah Shafiqah Haron and Nus'ha Azizan, for their tireless assistance and guidance. Special gratitude is reserved for my mother, Pn Zaniyah bt Ismail, whose unwavering support and encouragement have been instrumental in my journey. I owe my deepest gratitude to her for shaping me into the person I am today. I am also deeply grateful to my beloved wife, Ms. Rosatikah bt Rosli, for her unwavering love and support. I consider myself incredibly fortunate to have her in my life, and her presence has been a source of immense strength and joy. To my beloved children, Aufa Eryna, Nur Elisya, and Harith Elyas, you are my guiding lights and my greatest inspiration. I promise to do everything within my power to be the hero you deserve.

TABLE OF CONTENTS

ACKNOWLEDGEMENT ..... **ii**

TABLE OF CONTENTS ..... **iii**

LIST OF TABLES ..... **viii**

LIST OF FIGURES ..... **xi**

LIST OF SYMBOLS AND UNITS ..... **xv**

LIST OF ACRONYMS ..... **xix**

LIST OF APPENDICES ..... **xxii**

ABSTRAK ..... **xxiii**

ABSTRACT ..... **xxv**

CHAPTER 1 ..... **1**

1.1 Overview 1

1.2 Problem Statement 2

1.3 Research Objectives 5

1.4 Scope of Research 5

CHAPTER 2 ..... **7**

2.1 Graphene as Nanomaterial 7

2.1.1 Graphene Structure 8

2.1.2 Synthesis of Graphene and its Derivative 16

2.1.2(a) Mechanical Exfoliation 16

2.1.2(b) Chemical Exfoliation 18

2.1.2(c) Chemical Vapor Deposition 22

2.1.2(d) Chemical Synthesis 26

2.1.2(e) Reduction to RGO 29

2.1.3 Producing Graphene from Biomass 33

2.1.3(a) Thermal Treatment of Biomass 35

2.1.3(b) Exfoliation Method for Carbonized Biomass 40
2.1.4 Types of Agricultural Wastes Suitable for BG Production..... 42
2.1.5 Lignin as Raw Material for Bio-based Graphene 48
2.2 Drilling Activity in the Oil and Gas Industry..... 51
2.2.1 Types of Drilling Fluids..... 53
2.2.2 Water-based Drilling Mud 56
2.2.3 Nanoparticle in Drilling Operation 58
2.2.4 Non-Newtonian Fluid 60
2.3 Graphene and its Derivatives in the Oil and Gas Industry..... 62
2.3.1 Fluid Loss Additive..... 64
2.3.2 Permeability of the Mud Cake 65
2.4 Corrosion in Drilling Operation 69
2.4.1 Corrosion Inhibitors in Drilling 74
2.4.2 Weight Loss Study..... 77
2.5 Research Gap..... 79
CHAPTER 3 81
3.1 Overview 81
3.2 Chemicals..... 83
3.3 Apparatus 84
3.3.1 Pulping Machine 84
3.3.2 Centrifuge..... 84
3.3.3 Furnace..... 84
3.3.4 Homogenizer..... 85
3.3.5 Sonicator 85
3.3.6 Freeze-Dryer 85
3.3.7 Hamilton Mixer..... 85
3.3.8 Mud Balance 85

3.3.9 Viscometer 86
3.3.10 Low-Pressure Low-Temperature Filter Press 86
3.3.11 High-Pressure High-Temperature Filter Press 86
3.3.12 Grinder 86
3.3.13 Rolling Oven 87
3.4 Lignin Extraction 87
3.4.1 Converting the Oil Palm Biomass to Black Liquor 87
3.4.2 Converting Black Liquor to Lignin Powder 87
3.4.3 Lignin Purification 88
3.5 Bio-Graphene Exfoliation 88
3.5.1 Pre-treatment of Lignin Powder 88
3.5.2 Converting Pre-Treated Lignin to Carbonized Lignin 89
3.5.3 Exfoliation of Carbonized Lignin to Bio-Based Graphene Oxide 90
3.5.4 Exfoliation of Carbonized Lignin to Bio-Graphene 92
3.6 Characterization of Bio-Graphene 92
3.6.1 Characterization of Graphene Oxide Using Ultraviolet-Visible Spectroscopy 92
3.6.2 Characterization of Bio-Graphene Using Thermogravimetric Analyzer 92
3.6.3 Characterization of Bio-Graphene Using Raman Spectroscopy 93
3.6.4 Characterization of Bio-Graphene Using Fourier-Transform Infrared Spectroscopy 93
3.6.5 Characterization of Bio-Graphene Using Transmission Electroscopy Microscopy 93
3.6.6 Characterization of Bio-Graphene Using Atomic Force Microscopy 94
3.6.7 Characterization of Bio-Graphene Using X-Ray Photoelectron Spectroscopy 94
3.7 Water-Based Drilling Mud Formulation 94
3.7.1 Preparing Mud Formulation 94

3.7.2 Measuring the Rheology of the Mud Formulation 96

3.8 Fluid Loss Study Using Bio-Graphene as Additive in the Mud Formulation 97

3.8.1 Measuring Fluid Loss Using Low-Pressure Low-Temperature Filter Test 97

3.8.2 Measuring Fluid Loss Using High-Pressure High-Temperature Filter Test 98

3.8.3 Measuring Mud Permeability 99

3.9 Corrosion Study Using Benzimidazole as Additive in the Mud Formulation 99

3.9.1 Measuring Weight Loss Using Mud Formulation Containing Benzimidazole 100

3.9.2 Characterization of Carbon Steel Coupon Using Scanning Electron Microscopy-Energy Dispersive X-ray 101

3.10 Optimization of Mud Formulation 102

3.10.1 Taguchi Method 102

3.10.2 Measuring the Signal-to-Noise Ratio 103

3.10.3 Measuring Analysis of Variance 105

3.10.4 Grey Relational Analysis 106

CHAPTER 4 108

4.1 Optimal Thermal Treatment for Lignin Carbonization Process 108

4.2 Exfoliation of Bio-Graphene 115

4.2.1 Characterization of Bio-Graphene using Thermogravimetric Analyzer 116

4.2.2 Characterization of Bio-Graphene using Raman Spectroscopy ... 118

4.2.3 Characterization of Bio-Graphene using Fourier-Transform Infrared 121

4.2.4 Characterization of Bio-Graphene using Transmission Electron Microscopy 123

4.2.5 Characterization of Bio-Graphene using Atomic Force Microscopy 126

4.2.6 Characterization of Bio-Graphene using X-Ray Photoelectron Spectroscopy 127

4.3 Water-based Mud Formulation 129

4.3.1 Water-based Mud's Density and pH 130

4.3.2 Rheology Behaviour of Water-based Mud Formulation 134

4.4 Bio-Graphene as a Fluid loss additive 137

4.4.1 Effect of Bio-Graphene on the Rheology Behaviour 138

4.4.2 Effect of Bio-Graphene on Low-Pressure Low-Temperature Filtration test 141

4.4.3 Effect of Bio-Graphene on High-Pressure High-Temperature Filtration Test 143

4.4.4 Effect of Bio-Graphene on the Mud Cake 146

4.4.5 Overview of Bio-Graphene as a Filter Loss Additive in Water-based Mud 150

4.4.6 Comparing Bio-graphene Performances to Other Graphene Derivatives as a Fluid Loss Additive in Water-based Mud 151

4.5 Benzimidazole as Corrosion Inhibitor Additive 152

4.5.1 Effect of Benzimidazole on Weight Loss Study 154

4.6 Formulation Based on the Taguchi Method as a Design of Experiment 163

4.6.1 Optimization for Fluid Loss using The Taguchi Method 165

4.6.2 Optimization for Corrosion Mitigation using The Taguchi Method 173

4.6.3 Optimization for Viscosity using The Taguchi Method 179

4.6.4 The Significant of the Taguchi Method 184

4.7 Formulation Based on Grey Relational Analysis 186

4.8 Chapter Summary 191

CHAPTER 5 194

5.1 Conclusions 194

5.2 Future Recommendations 196

REFERENCES 198

APPENDICES

LIST OF TABLES

Page

Table 2.1 List of chemical exfoliation methods with the help of the sonicator 20

Table 2.2 Graphene CVD recipes on primary metal substrates 24

Table 2.3 List of modified Hummers methods 28

Table 2.4 Reducing methods by using acid and metal 30

Table 2.5 Reducing methods by using alkali and metal 32

Table 2.6 The pre-treatments and processes to convert biomass to BG 43

Table 2.7 Some of the mud formulation components [185] 58

Table 2.8 List of materials used and their characteristics as drilling pipe and casing [218] 70

Table 2.9 Possible sources of corrosion contaminants during the drilling operation [217] 72

Table 2.10 Example of mud formulation for water-based and oil-based drilling mud [232] 77

Table 3.1 Proximate analysis of OPEFB [234] 83

Table 3.2 The parameter for thermal treatment of pre-treated lignin 90

Table 3.3 Components for mud formulation 95

Table 3.4 Various concentrations of BG for the fluid loss test 97

Table 3.5 Various concentrations of BI for the corrosion study 100

Table 3.6 The parameters for 3 levels of control factors 102

Table 3.7 List of trial run numbers and the control factors 103

Table 4.1 Raman spectra reading for BG, Commercial graphene, and CL 119

Table 4.2 List of IR spectrum absorption frequency for GO and BG particle .123

Table 4.3 XPS peak deconvolution break down 129

Table 4.4 Preliminary WBM formulation for 8 wt% of bentonite.....130
Table 4.5 Mud weight for various mud formulation.....131
Table 4.6 Rheology properties of mud formulation.....137
Table 4.7 Density and pH values of mud formulation with BG 139
Table 4.8 Rheology properties of Mud formulation with various BG concentrations 140
Table 4.9 Comparison of API filter-loss reducer performances of various BG concentrations 142
Table 4.10 A comparison LPLT filter loss study of graphene derivatives in WBM.....142
Table 4.11 Comparison of HPHT filter test for various BG concentration 145
Table 4.12 A comparison HPHT fluid loss study of graphene derivatives in WBM.....145
Table 4.13 The weight loss results after rolling oven simulation at 100 °C 156
Table 4.14 Elements composition of SEM images 160
Table 4.15 List of the control factors and responses.....163
Table 4.16 Raw materials for the mud formulation based on the mixing time..164
Table 4.17 The list of responses and their preferred design.....165
Table 4.18 The response and S/N values for API fluid loss study based on the L-9 trial runs.....166
Table 4.19 The M_{AVG} and the delta values for fluid loss optimization.....170
Table 4.20 The ANOVA and pooled ANOVA based on the S/N of the fluid loss response 171
Table 4.21 Optimum mud formulation conditions for fluid loss and its predicted response.....172
Table 4.22 The response and S/N values for the weight loss study based on the L-9 trial runs.....174
Table 4.23 The M_{AVG} and the delta values for weight loss optimization.....176

Table 4.24 The ANOVA and pooled ANOVA based on the S/N of the weight loss response 177

Table 4.25 Optimum mud formulation conditions for weight loss and its predicted response 178

Table 4.26 The response and S/N values for the weight loss study based on the L-9 trial runs 180

Table 4.27 The M_{AVG} and the delta values for viscosity optimization 183

Table 4.28 The ANOVA and pooled ANOVA based on the S/N of the viscosity response 184

Table 4.29 Optimum mud formulation conditions for viscosity and its predicted response 184

Table 4.30 List of optimum mud formulations for different responses 185

Table 4.31 S/N value, normalized S/N, and the delta values for each trial runs 188

Table 4.32 Grey coefficient based on the S/N values for each trial 189

Table 4.33 Mean response table for the grey relational grade 190

Table 4.34 Summary of the results and discussion 191

LIST OF FIGURES

Page

Figure 2.1 Graphene, GO, and RGO structures [17] 7

Figure 2.2 Atomic orbital diagram of a carbon atom. The four electrons in the 2s orbital and 2p orbitals hybridized to form sp^2 orbitals as in graphene [25] 10

Figure 2.3 Carbon atoms bonded with a bond length of 0.142 nm in a honeycomb lattice [23] 10

Figure 2.4 Allotropes of carbon from basic structure of (a) graphene gives us (b) fullerenes, (c) carbon nanotubes and d) graphite [27] 12

Figure 2.5 Graphene defects (a) intrinsic defect and (b) extrinsic defects [29] .. 12

Figure 2.6 The illustration of multilayer structure for (a) AA stack, (b) AB stack, and (c) twisted layer with θ angle [32] 14

Figure 2.7 Band structure for pristine graphene and multilayer graphene [30] .. 15

Figure 2.8 Mechanical routes using sheer force to separate graphene layers [38] 17

Figure 2.9 Electrochemical method of graphite used as electrode resulting in graphene flakes deposited into the electrolyte [47] 19

Figure 2.10 Schematic of the graphene CVD mechanism [61] 23

Figure 2.11 The routes of converting biomass into carbon-related materials [114] 35

Figure 2.12 Illustration of the re-arrangement of the carboneous material to form graphite-like structure [2] 37

Figure 2.13 The major phenylpropanoid monomers and the most common inter-unit linkage of lignin [162] 49

Figure 2.14 The drilling base for the offshore operation consists of conductor pile, casing, drill string and the drill bit [171] 53

Figure 2.15 Types of drilling fluid in the oil and gas industry [172] 54
Figure 2.16 Statistical research articles published for nano drilling fluid from 2000 to 2022. Source: Scopus.....59
Figure 2.17 Comparison of the Herschel-Bulkley model and the Bingham plastic model [195].....61
Figure 2.18 Schematic diagram for API fluid loss test [210].....67
Figure 2.19 Types of corrosion inhibitors used in the oil and gas industry [213] 73
Figure 2.20 Type of corrosion (a) uniform corrosion, (b) pitting corrosion, (c) crevice corrosion, and (d) galvanic corrosion [213] 74
Figure 2.21 Illustration of organic corrosion inhibitor absorbed onto the metal surface, forming a barrier [228] 76
Figure 3.1 The research workflow.....82
Figure 3.2 The apparatus set up for the ice bath in preparing the GO.....91
Figure 3.3 The illustration of preparing the mud formulation.....95
Figure 4.1 Precipitate SL versus pH value 110
Figure 4.2 TGA analysis of the SL sample 111
Figure 4.3 The percentage of CL yield versus temperature 112
Figure 4.4 The UV spectra of GO exfoliated from CL300, CL600, CL800, and CL1000.....114
Figure 4.5 Proposed mechanism of the formation of BG particle.....116
Figure 4.6 TGA analysis for CL800.....117
Figure 4.7 TGA analysis for BG 118
Figure 4.8 Raman spectroscopy comparing BG, commercial graphene, and CL.....120
Figure 4.9 The FTIR spectra of BG, GO, and the commercial graphene.....122
Figure 4.10 TEM images for BG particles with a scale bar of 50 nm.....125
Figure 4.11 Size distribution for BG particle based on the TEM image.....125

Figure 4.12 BG thickness identification using AFM.....126

Figure 4.13 (a) XPS survey spectra, (b) high-resolution XPS spectra of C 1s region, and (c) high-resolution XPS spectra of O 1s region of the BG particle.....128

Figure 4.14 The mud balance reading scale. 132

Figure 4.15 XRD analysis for Bentonite 133

Figure 4.16 Shear stress vs. shear rate plots of WBM (water + bentonite + Na_2CO_3) 136

Figure 4.17 Stability study of A (BG) and B (CL) in water after 1h of sonication 138

Figure 4.18 Shear stress vs. shear rate plots of WBM with various BG concentrations 140

Figure 4.19 API (LPLT) fluid loss versus time for different BG concentrations 143

Figure 4.20 HPHT fluid loss versus time for various BG concentrations.....146

Figure 4.21 Mud cake collected after API filter test for (a) blank mud formulation and (b) MF-BG4 and after HPHT filter test for (c) blank and (d) MF-BG4.....148

Figure 4.22 SEM images of mud cake (a) blank and (b) MF-BG4.....149

Figure 4.23 Schematic diagram of the mechanism that involves BG in the drilling mud.....149

Figure 4.24 Mud cake permeability of API and HPHT fluid test for various BG concentration.....150

Figure 4.25 TGA thermogram for BI and inside is the structure for BI.....153

Figure 4.26: The carbon steel coupon surface (a) before being immersed in the WBM, (b) after being in the WBM without BI, and (c) after being immersed in WBM with BI.....155

Figure 4.27 The effect of BI concentration in WBM versus (a) corrosion rate and (b) inhibitor efficiency.....157

Figure 4.28 The SEM images and the EDX spectrum of the carbon steel coupon; (a) polished-before screening, (b) without BI, and (c) 500 ppm BI.....159

Figure 4.29 Langmuir plot of BI on carbon steel corrosion in mud formulation 162

Figure 4.30 Temkin plot of BI on carbon steel corrosion in mud formulation ...162

Figure 4.31 The main effects plot for the fluid loss response 167

Figure 4.32 The mud formulation (a) in a normal situation while (b) and (c) represent bubble effect plagues the mud.....168

Figure 4.33 The mud cake thickness with varying bentonite concentration 169

Figure 4.34 The actual versus prediction graph for the fluid loss response 173

Figure 4.35 The main effects plot for the weight loss response.....176

Figure 4.36 The actual versus prediction graph for the weight loss response.....179

Figure 4.37 The main effects plot for viscosity response.....182

Figure 4.38 Mean graph for the grey relational grade.....191

LIST OF SYMBOLS AND UNITS

$	United States dollar
%	Percentage
°C	Degree Celsius
°C min^{-1}	Degree Celcius per minute
°F	Degree Fahrenheit
µm	Micrometre
Å	Angstrom
At.%	Atomic percent
atm	Standard atmosphere
BH^{4-}	Borohydride ion
BI	Benzimidazole
CH_4	Methane
ClO_2	Chlorine dioxide
cm	Centimetre
cm^{-1}	Reciprocal wavelength
CO_3^{-2}	Carbonate ions
cP	Centipoise
eV	Electron volt
$Fe(OH)_2$	Iron (II) hydroxide
$FeCl_2$	Iron (II) chloride
g	Gram
g L^{-1}	Gram per litre
H_2CO_3	Carbonic acid

H_2O	Water
H_2O_2	Hydrogen peroxide
H_2S	Hydrogen sulfide
H_2SO_4	Sulfuric acid
H_3O^+	Hydronium ion
H_3PO_4	Phosphoric acid
HCl	Chloric acid
HCO^{3-}	Bicarbonate ions
HeNe	Helium-neon
HF	Hydrofuran
HNO_3	Nitrate acid
hr	Hour
Hz	Hertz
K_2FeO_4	Potassium ferrite
$K_2S_2O_8$	Potassium persulfate
KBr	Potassium bromide
$KClO_3$	Potassium chlorate
kg L^{-1}	Kilogram per litre
kHz	Kilohertz
$KMnO_4$	Potassium permanganate
KOH	Potassium hydroxide
kPa	Kilopascal
L	Litre
lb $100ft^{-2}$	Pounds per hundred square feet
lb bbl^{-1}	Pounds per barrel

lb gal^{-1}	Pounds per gallon
mg	Miligram
mg	Miligram
min	Minute
mL	Mililitre
mL min^{-1}	mililitres per minute
mm	Milimetre
mm y^{-1}	Milimetre per year
MMscf D^{-1}	Million standard cubic feet per day
MnO_2	Manganese dioxide
mW	Miliwatts
Na_2CO_3	Sodium carbonate
Na_2CO_3	Sodium carbonate
$NaBH_4$	Sodium borohydride
$NaNO_3$	Sodium nitrate
NaOH	Sodium hydroxide
NH_3BH_3	Ammonia borane
NH_4OH	Ammonium hydroxide
nm	Nanometer
O_3	Ozone
OH^-	Hydroxide ion
P_2O_5	Phosphorus pentoxide
Pa	Pascal
Pa s^{-1}	Pascals per second
ppb	Part per billion

ppg	Pounds per gallon
ppm	Part per million
psi	Pounds per square inch
RM	Ringgit Malaysia
rpm	Revolutions per minute
s	Second
s^{-1}	Reciprocal of seconds
sccm	Standard cubic centimetre per minute
t	Tonne
v/v	Volume per volume
W	Watt
w/v	Weight per volume
wt%	Weight percent

LIST OF ACRONYMS

%IE	Inhibitor efficiency percentage
0D	Zero dimensional
2D	Two dimensional
3D	Three dimensional
ABS	Copolymer of acrylonitrile, butadiene, and styrene
AFM	Atomic force microscopy
ANOVA	Analysis of variance
AP	Apparent viscosity
API	American Petroleum Institute
ASTM	American Society for Testing and Materials
B/RGO	Boron-doped RGO
BG	Bio-based graphene
B-GO	Bio-based GO
C/O	Carbon to oxygen ratio
CAS	Chemical abstracts service
C_{inh}	Inhibitor concentration
CL	Carbonized lignin
CMC	Carboxymethyl cellulose
CNT	Carbon nanotubes
CR	Corrosion rate
CVD	Chemical vapor deposition
DNA	Deoxyribonucleic acid
DOE	Design of experiments
DOF	Degree of freedom
EFB	Empty fruit bunches
F	Variance ratio
FTIR	Fourier Transform Infrared
FWHM	Full-width at half-maximum
GNP	Graphene nanoparticle
GO	Graphene oxide
GO-NS	Graphene oxide nanostructure

HPHT	High-pressure high-temperature
HTC	Hydrothermal carbonization
I_{2D}	2D band intensity
I_G	G band intensity
ISO	Interational Organization for Standard
KL	Kraft lignin
LFGO/PGO	Large flake graphene oxide/powder graphene oxide
LPLT	Low-pressure low-temperature
LT-CVD	Low temperature CVD
M_{AVG}	Mean of S/N
M_B	S/N value relative to factor
MWCNT	Multi-walled carbon nanotubes
NORSOK	Norsk Sokkels Konkurranseposisjon
NO_x	Nitrogen oxide gasses
PAAN/G	Acrylamide polymer/graphene oxide composite
PAC	Polyanionic cellulose
PV	Plastic viscosity
PVC	Polyvinyl chloride
PVP	Polyvinylpyrrolidone
RGO	Reduced graphene oxide
RT	Room temperature
RT-CVD	Rapid thermal CVD
S	Sum of square
S/N	Signal-to-noise ratio
S’	Adjusted sum of square
Sdn Bhd	Sendirian Berhad
SDOC	Sodium deoxycholate
SDS	Sodium dodecyl sulfate
SEM	Scanning electron microscopy
SL	Soda lignin
SWCNT	Single-walled carbon nanotubes
T-CVD	Thermal CVD
TEM	Transmission electron microscopy
TGA	Thermogravimetric analysis

THF	Tetrahydofuran
UHV-CVD	Ultra-high vacuum CVD
UV	Ultra-violet
UV-Vis	Ultraviolet-visible spectroscopy
V	Variance
WBM	Water-based drilling mud
XPS	X-ray photoelectron spectroscopy
XRD	X-ray diffraction
YP	Yield point

LIST OF APPENDICES

APPENDIX A DATA AND CALCULATIONS

APPENDIX B NOVELTY STUDIES

APPENDIX C ACHIEVEMENTS

APPENDIX D LIST OF PUBLICATIONS AND PATENTS

GRAFENA BERASASKAN BIO DARI TANDAN KELAPA SAWIT SEBAGAI BAHAN TAMBAH UNTUK MENGURANGKAN KEHILANGAN CECAIR BAGI LUMPUR GERUDI BERASASKAN AIR

ABSTRAK

Salah satu masalah serius yang dihadapi semasa operasi pengerudian ialah kehilangan bendalir gerudi meresap kedalam dinding telaga, yang dirujuk sebagai kehilangan bendalir, yang akan mengakibatkan bendalir gerudi kering lalu mengakibatkan gerudi tersekat. Untuk mengatasi kejadian tersebut, bahan tambahan kehilangan bendalir ditambah ke dalam bendalir gerudi. Keberkesanan grafena berasaskan bio (BG) yang disediakan daripada biomas tandan kelapa sawit (*Elaeis guineensis*) sebagai bahan tambah untuk mengurangkan kehilangan cecair bagi lumpur gerudi berasaskan air (WBM) telah dikaji. BG telah dieksfoliasi daripada lignin yang diekstrak melalui proses pempulpaan soda. Proses eksfoliasi BG terdiri daripada gabungan rawatan haba melalui pirolisis pada suhu 300, 600, 800, dan 1000 °C dengan masa tindak balas selama 60 minit di dalam gas argon, diikuti dengan eksfoliasi secara mekanikal menggunakan penghomogen dengan kelajuan ricih 12400 rpm selama 1 jam. Spektroskopi ultralembayung-cahaya nampak (UV-Vis), analisis terma gravimetrik (TGA), spekrtoskopi transformasi inframerah Fourier (FTIR), spektroskopi Raman, mikroskop elektron penghantaran (TEM), mikroskop pengimbasan elektron (SEM), mikroskopi daya atom (AFM), and spektroskopi fotoelektron sinar-x (XPS) digunakan untuk mencirikan setiap sampel yang disediakan. Analisis Raman mengesahkan pembentukan grafena berdasarkan nilai I_{2D}/I_G yang menyerupai graphene komersial, iaitu 0.91. Analisis FTIR mendedahkan bahawa struktur BG mempunyai jumlah kumpulan berfungsi kurang daripada GO,

yang telah disahkan menggunakan XPS berdasarkan nisbah C/O BG kurang daripada GO. Analisis UV-Vis mendedahkan bahawa suhu rawatan terma optimum ialah pada suhu 800 °C dengan keamatan tinggi berhampiran 220 nm. Untuk menilai kehilangan bendalir, ujian penapis tekanan rendah suhu rendah (LPLT) dan ujian penapis tekanan tinggi suhu tinggi (HPHT) telah dijalankan. Menurut ujian penapis LPLT, 0.5 wt% BG menyebabkan kehilangan bendalir paling sedikit pada 10 ml selama 30 minit, tetapi ujian penapis HPHT menunjukkan bahawa 1.0 wt% BG menyebabkan kehilangan bendalir paling sedikit pada 18 ml selama 30 minit. Kesan BG sebagai tambahan lumpur gerudi adalah setanding dengan grafena komersial yang dilaporkan dalam penyiasatan awal, dilaporkan memperoleh pengurangan sebanyak 50% dalam kehilangan bendalir dan morfologi permukaan lumpur yang berbeza dengan struktur yang kurang berpori dan permukaan yang lebih licin, oleh itu, kurang tulus. Dengan menggunakan kaedah Taguchi dan analisis hubungan Grey, parameter optimum untuk rumusan lumpur ditentukan, dengan menjadikan prestasi pengurangan kehilangan bendalir, prestasi perencatan kakisan dan kelikatan sebagai tindak balas. Berdasarkan analisis berbilang tindak balas, formulasi optimum bagi lumpur ialah 0.5 wt% BG, 5 wt% benzimidazole (BI), 60 minit masa bancuhan, dan 8 wt% bentonit.

BIO-BASED GRAPHENE FROM THE OIL PALM EMPTY FRUIT BUNCHES AS A FLUID LOSS ADDITIVE IN THE WATER-BASED DRILLING MUD

ABSTRACT

One of the most serious issues encountered during drilling operations is the loss of drilling fluid through the well formation, which is referred to as fluid loss, resulting in dry drilling fluid and increasing the likelihood of the drill being stuck. To prevent this scenario, a fluid loss additive was added to the drilling mud. The effectiveness of bio-based graphene (BG) prepared from oil palm (*Elaeis guineensis*) empty fruit bunches biomass as a fluid loss additive for water-based drilling mud (WBM) was investigated. To accomplish this, BG was exfoliated from lignin extracted through a soda pulping process. The BG exfoliation process consisted of a combination of thermal treatment *via* pyrolysis at 300, 600, 800, and 1000 °C with a reaction time of 60 minutes under an argon atmosphere, followed by a mechanical exfoliation using a homogenizer with a shear rate of 12400 rpm for 1 hour. Ultraviolet-visible spectroscopy (UV-Vis), thermogravimetric analysis (TGA), Fourier-transform infrared spectroscopy (FTIR), Raman spectroscopy, transmission electron microscopy (TEM), scanning electron microscopy (SEM), atomic force microscopy (AFM), and x-ray photoelectron spectroscopy (XPS) were used to characterize each prepared sample. The Raman analysis confirmed the graphene formation based on the I_{2D}/I_G value similar to the commercial graphene, i.e., 0.91. The FTIR analysis revealed that the BG structure has a less functional group than GO, which has been confirmed using XPS as the C/O ratio of BG is less than GO. The UV-Vis analysis revealed that the optimal thermal treatment temperature is 800 °C with a high intensity near 220 nm. To

assess the fluid loss, a low-pressure low-temperature (LPLT) filter test, and a High-Pressure High-Temperature (HPHT) filter test were performed. According to the LPLT filter test, 0.5 wt% BG caused the least fluid loss at 10 ml for 30 minutes, but the HPHT filter test indicated that 1.0 wt% BG caused the least fluid loss at 18 ml for 30 minutes. The efficacy of BG as a drilling mud addition is comparable to that of commercial graphene reported in earlier investigations, as shown by the 50 % reduction in fluid loss and noticeable different surface morphology of the mud cake with less porous structure and smoother surface, therefore less permeability. Using the Taguchi method and Grey relational analysis, the optimal parameter for the mud formulation was determined, with the fluid loss reducer performance, corrosion inhibition performance, and viscosity as the responses. Based on the multi-response analysis, the optimal formulation conditions for mud are 0.5 wt% of BG, 5 wt% of benzimidazole (BI), 60 minutes of mixing time, and 8 wt% of bentonite.

CHAPTER 1

INTRODUCTION

1.1 Overview

Graphene is considered the material of the future due to its exceptional qualities and has been developed for some time. However, it is rarely accessible due to its prohibitive cost. Alternatives have been designed as a remedy by utilizing an effective method to reduce manufacturing costs while improving production output is one of these methods. Another greener solution is to use less expensive raw materials such as biomass. Producing graphene from biomass, or bio-based graphene (BG), has been attempted as a solution for producing graphene in a more sustainable manner. Biomass can be transformed into graphene in two steps [1]. The initial step is a thermal treatment followed by an exfoliation technique. Thermal treatment is a typical pyrolysis technique utilized by numerous businesses to transform biomass into bio-oils, biogas, and bio-char. Through the exfoliation process, biochar can be transformed into graphene. Hummers method is a standard bio-char exfoliation approach based on an oxidation process. The disadvantage of this approach is that it converts biochar to graphene oxide (GO) by introducing oxygen-containing functional groups into the lattice, necessitating a further purification step *via* a reduction process to turn it into BG [2]. This study offered a unique BG conversion using the homogenizer and sonicator mechanical exfoliation technique. This chapter includes background information, the purpose of the research, the explanation of the problem, the research objectives, and the scope of the investigation.

1.2 Problem Statement

One of the most serious issues encountered during drilling operations is the loss of drilling fluid through the well formation, referred to as fluid loss. As a result, the drilling fluid will dry and become more viscous, putting greater strain on the drill bit and increasing the likelihood of the drill being stuck. Another major issue is when dehydrated mud or mud cake adheres to the formation, lowering the volume of the annulus gas and thus increasing the pressure inside the formation. An uncontrollable well with bad practical procedures will lead to the mud sneaked into the annulus, resulting in the formation pressure is higher than the wellbore pressure or known as kicks and blowouts. These incidents occurred worldwide during the drilling operation, which has cost lots of life, as reported by Ashena et al. [3]. A thick filter cake will jam the driller's pipes, causing drag and torque difficulties. A considerable volume of fluids penetrating a porous rock formation would eventually cause the wellbore to collapse, in addition to changing the rheology and physical properties of the drilling fluid [4].

To address this issue, a fluid loss additive will be added *via* forming a mud cake with low permeability and low thickness around the wellbore. There are other drilling fluid loss additives available on the market; however, none can outperform a nanoparticle fluid loss capability due to its having a higher surface-to-volume ratio than the other two. The capacity of nanoparticles to penetrate the formation and create an interior layer to effectively construct a low permeability filter, thereby sealing the formation, is fundamental to their success as a fluid loss enhancer [5].

Even though graphene exceptionally performs well as a fluid loss additive, it is rarely accessible due to its low cost and yield efficiency [6]. The production of pristine graphene is arduous, with low yield, resulting in a very costly production cost. As a result, graphene faces a sluggish expansion in the market due to the limited

manufacturing of graphene, which has caused the sector to seek alternatives or utilize the current material. Although graphene technology has advanced significantly since its initial discovery, the production cost is still too high to warrant a move since the current price for 500 mg of pure graphene exceeds RM 2,000 [7]. In addition, the initial expense of creating graphene stems from the cost of the raw material. A normal route in producing graphene is by exfoliating graphite. Although graphite is very inexpensive (RM 400 per kilogram), graphene production has a low yield, making the process expensive.

In 2018, the oil palm sector made a significant contribution of approximately 2.8 % (RM 37.71 billion) to Malaysia's GDP. Additionally, in 2019, the sector provided employment opportunities for up to 400 thousand individuals, that expected to rise annually [8]. The oil palm industry's farming practices resulted in the majority of oil palm waste (primarily tree trunks, fronds, empty fruit bunches (EFB), and shells) being left to degrade in the fields. Although decomposed biomass is a valuable source of fertilizer, it has been noted that the biomass causes significant fungal growth at the roots of oil palm trees [9]. In accordance with the greener policies enforced in most developed countries, greener graphene was deemed necessary. Graphene can be made from biomass by concentrating the carbon elements in the structure while eliminating the majority of other elements through thermal processing.

The lignocellulosic components of biomass are cellulose, hemicellulose, and lignin. When the temperature hits 200 °C, the three lignocellulosic materials begin to break down, releasing tiny molecular weight components [10]. Biomass has been utilized as the carbon source in the CVD process in combination with graphite and other gaseous materials [11]. For pyrolysis conversion, it was found that lignin provides the most graphitized carbon structure in the form of bio-char as lignin is rich

with phenolic components, while other lignocellulosic materials formed bio-oils and bio-gaseous [12]. Lignin has been considered a waste by-product in the paper industry, and utilizing only lignin as the raw material for graphene production is the best approach to solve waste management and create greener graphene.

1.3 Research Objectives

The present study concentrates on preparing bio-based graphene (BG) from lignin which was extracted from oil palm EFB. Therefore, the research objectives are as follows:

1. To synthesize BG from oil palm EFB's lignin through a novel mechanical exfoliation technique.
2. To characterize the BG using FTIR, UV-Vis, TGA, TEM, Raman, AFM, and XPS, while comparing it to the commercial graphene.
3. To determine the effectiveness of BG as a fluid loss additive in WBM.
4. To optimize the BG formulation in WBM using Taguchi method and Grey relational analysis.

1.4 Scope of Research

The scope of this study is divided into 4 stages based on research objectives. The first stage is to prepare the BG from the lignin of oil palm EFB. Two-step processes were carried out in order to convert lignin into BG. The first step is a thermal treatment, where the lignin is subjected to high temperatures to concentrate the carbon content in the lignin structure. The second step is mechanical exfoliation using a homogenizer and a sonicator. UV-Vis analysis is used to determine the optimum thermal temperature for the process. The second stage of this study is the characterization process to compare BG with commercial graphene. It is essential that the BG particle size is identified and checked *via* TEM, as the third stage is the utilization of BG as a fluid loss additive in WBM. The third stage involved a formulation of BG in the WBM. The rheology test is carried out based on the API standard involving the viscosity, density, API, and HPHT Filter Press. The performance of BG as fluid loss additive will be compared to other graphene data

available in the literature. The final/fourth stage of this study is to optimize the formulation of BG in WBM. This stage was set up to identify BG behaviour when mixing with other additives. Weight loss analysis for measuring corrosion inhibitor properties is used to determine BG's influence on benzimidazole as a corrosion inhibitor. The optimization design used for this study is the Taguchi method and Grey relational analysis. Details explanation of the scope of the study are as follows:

CHAPTER 2

LITERATURE REVIEW

2.1 Graphene as Nanomaterial

Graphene is an allotrope of carbon made up of a single layer of sp^2-bonded carbon-to-carbon atoms arranged in a hexagonal lattice [13]. Graphene can be found in most of the carbon's structural family, as the graphene sheet is the building structure for all other carbon arrangements. Graphene started with a theory that an atom-thick graphite film will possess the flexibility and strength to bend, roll, and fold. Nonetheless, the notion of an individual 2D structure was considered far-fetched because of its unstable condition to retain its structure. However, in 2004, when a group of researchers from Manchester could extract and characterized graphene [14]. The reason for all the publicity related to graphene was its unique characteristics and high thermo-mechanical properties, which are becoming the most robust materials today [15]. Three types of derivatives represent the graphene group; pristine graphene, graphene oxide (GO), and reduced graphene oxide (RGO) (Figure 2.1).

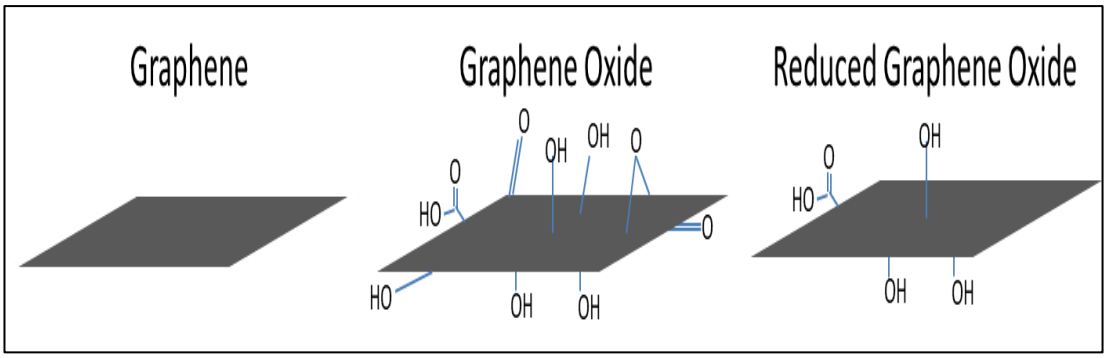

Figure 2.1 Graphene, GO, and RGO structures [16]

Graphene technology has existed since 2010, but its application in the nanotechnology market is still lacking. The transformation process of graphene production from laboratories to a large industrial scale was not linear. Although

graphene is mainly exfoliated from graphite, a sheet of high-quality graphene in the market can reach around 100 dollars per gram, even though graphite price is around 1 cent per gram [17]. Its high price is due to the difficulty in obtaining high-quality graphene, i.e., the processing and production costs. Furthermore, the production through exfoliation, chemical vapor deposition (CVD), epitaxial growth, etc., only yields a small amount of graphene. Although the conversion of graphene still leaves much to be desired, the graphene market is projected for steady growth because many companies are willing to participate in the graphene revolution [18].

Depending on the production method, graphene can be exfoliated as either a micromaterial or a nanomaterial. Micro-structured graphene, known as sheets (usually more than 200 nm), and nano-structured graphene, referred to as flakes (usually less than 100 nm), are the two primary forms [19]. Unless specified otherwise, graphene is typically produced in multiple sheets. For instance, Xin et al. fabricated porous graphene in sheets and employed it as a material for supercapacitors, demonstrating exceptional performance owing to its porous structure [20]. In that study, the researchers did not focus on the graphene size as it did not influence the outcome. Conversely, Gao et al. generated graphene flakes to investigate the impact of graphene size on asphalt performance [21]. They observed that the size of graphene significantly influenced the performance of modified asphalt.

2.1.1 Graphene Structure

Understanding the remarkable structure of graphene is equivalent to fully grasping the singularity of carbon as an atom and the entire family of carbon allotropes. As the element with the highest frequency of occurrence on Earth, carbon has the atomic number 6, and its electrons occupy the $1s^2$, $2s^2$, $2p_x^1$, and $2p_y^1$ orbitals. The differences in structure between graphene and graphite play a significant role in

graphene's unique properties. For example, graphite is known to be a good conductor of electricity, making graphite a common fabrication material for electrodes. This is due to delocalized electrons in the graphite's surface, which are easily transported across the plane but not in or through it [22]. Imagine if a structure is thin enough to enable the electron to move throughout the structure without limitation. That's graphene, which is why it offers such high electron mobility.

Figure 2.2 shows the sp^2 orbitals with three orbitals of hybridized 2s and 2p formed with 3 electrons filled up the hybridized, leaving 1 electron on the unhybridized 2p orbital. As the sp^2 orbitals constitute 33.3 percent of 2s orbital, the energy level is lower than the sp^3 orbital, which only constitutes 25 percent of 2s orbital. The hybridized orbital is aligned on the same basal plane, while the unhybridized 2p orbital is perpendicular to the plane. At 120° angles from each other, the bond formation will create a hexagonal or honeycomb-like structure [13]. Graphitic carbon is an example of the bonding structure of sp^2 carbon atoms. In each layer, the C-C bonds are settled in position with a separation of 0.142 nm (Figure 2.3), and the interspace between each plane (layers) is 0.335 nm [23]. The honeycomb or lamellar structures feature sturdier C-C bonds than those linking the layers. This is because the perpendicular π-bonds, formed by the remaining 2p orbitals, have significantly lower binding energy, which can lead to an easy shearing along the layer plane to separate layers of graphite into graphene [24].

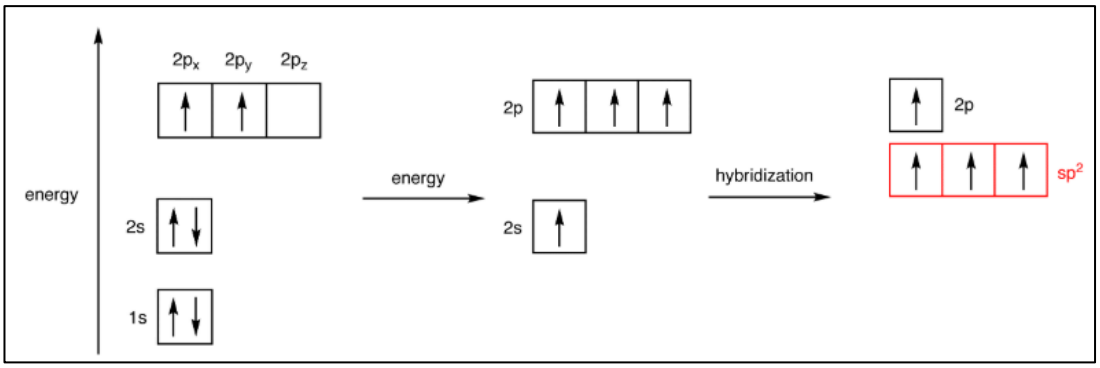

Figure 2.2 Atomic orbital diagram of a carbon atom. The four electrons in the 2s orbital and 2p orbitals hybridized to form sp^2 orbitals as in graphene [25]

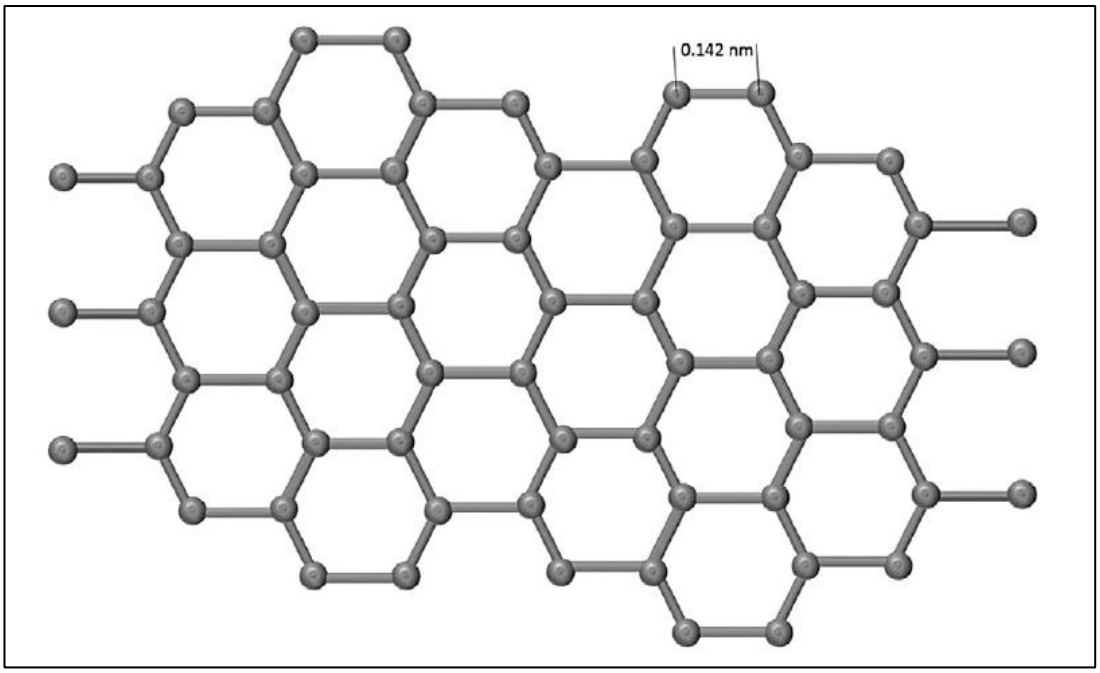

Figure 2.3 Carbon atoms bonded with a bond length of 0.142 nm in a honeycomb lattice [23]

Graphitic carbon groups include graphite, graphene, carbon nanotubes, graphyne, and several others [16], [26]. A layer of graphene is the basic structural element for other allotropes, such as graphite (3D graphene) and fullerene (0D graphene). Fullerenes, also known as buckyballs, was first uncovered in the middle of the 1980s. Carbon atoms are composed in hexagonal linkage at the primary core with the edge connected to form a globe-like structure, as shown in Figure 2.4.

Mechanically, fullerenes are proven to be extremely strong molecules, given their ability to resist tremendous pressures, as the hexagonal linkage retained the original structure even after being subjugated to over 3000 atm [27]. Another edge-to-edge graphene formation is carbon nanotube (CNT). CNT is a family of fullerenes having its owned unique properties associated with their molecular structure, which consists of 1) single-walled carbon nanotubes (SWCNT), composed of small diameters of one single hollow tube and 2) multi-walled carbon nanotubes (MWCNT) where it has more concentric tubes with different diameters. These two structures are essential for their electronic properties, as SWCNT can be semiconducting or metallic, while MWCNT can be only metallic [11].

There is a high chance that synthesized graphene may result in defective graphene. In fact, defective graphene is more common than pristine graphene as structural defects are common occurrences in carbon-based structures and have been studied before, especially for CNT and graphite [28]. There are two types of defects in graphene; intrinsic and extrinsic defects. Extrinsic defects are caused by unknown atoms intercalating on the surface of graphene. In contrast, intrinsic defects are caused by non-sp^2 orbitals of carbon atoms within the hexagonal structure, as shown in Figure 2.5. Ultimately, these imperfections will alter the structure and properties of graphene. In addition, research has demonstrated that defective graphene can either improve (thermal conductivity, electrochemical performance, and magnetic properties) or degrade (mechanical properties) graphene's properties. Therefore, based on the task, defective graphene can solely outperform pristine graphene. For example, in the manufacturing industry, defective graphene can be modified and regulated so that its ability fits the particular application, which speaks greatly to the adaptability of graphene as a whole.

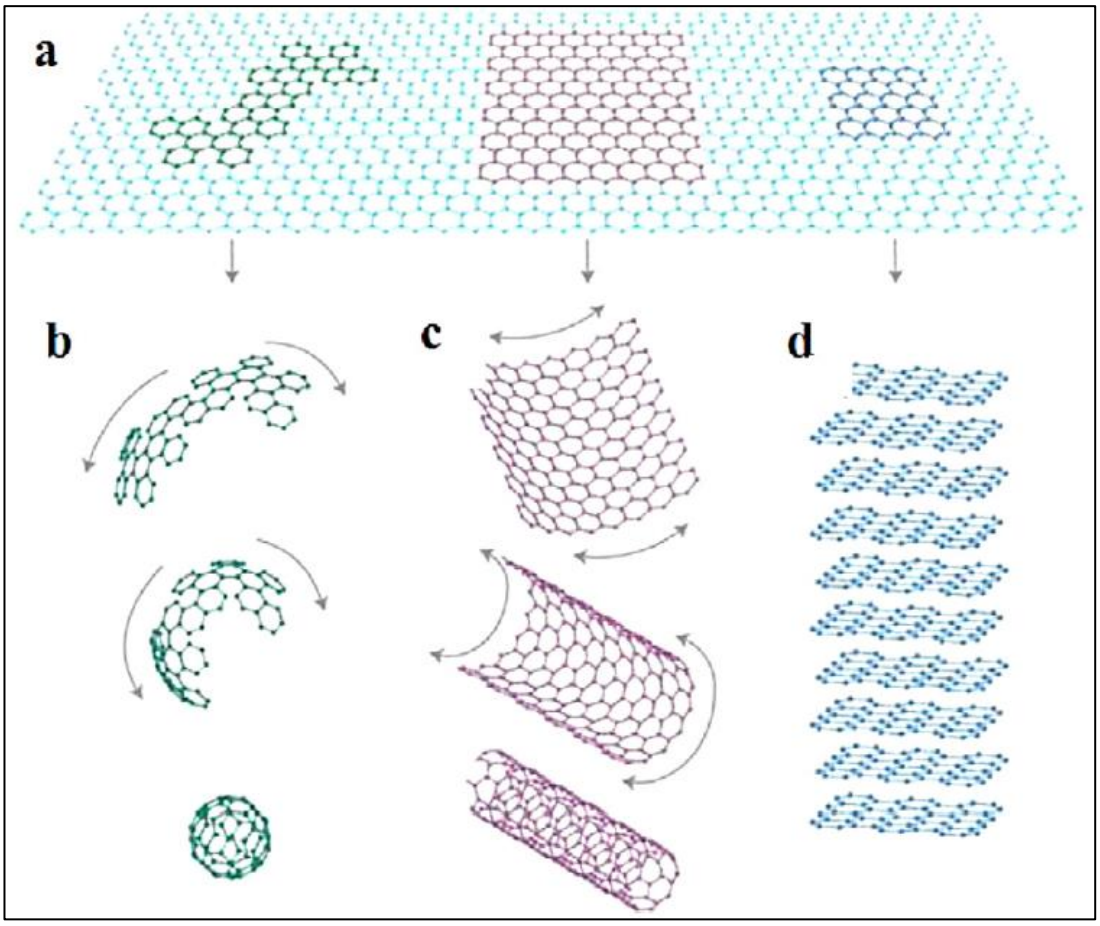

Figure 2.4 Allotropes of carbon from basic structure of (a) graphene gives us (b) fullerenes, (c) carbon nanotubes and d) graphite [27]

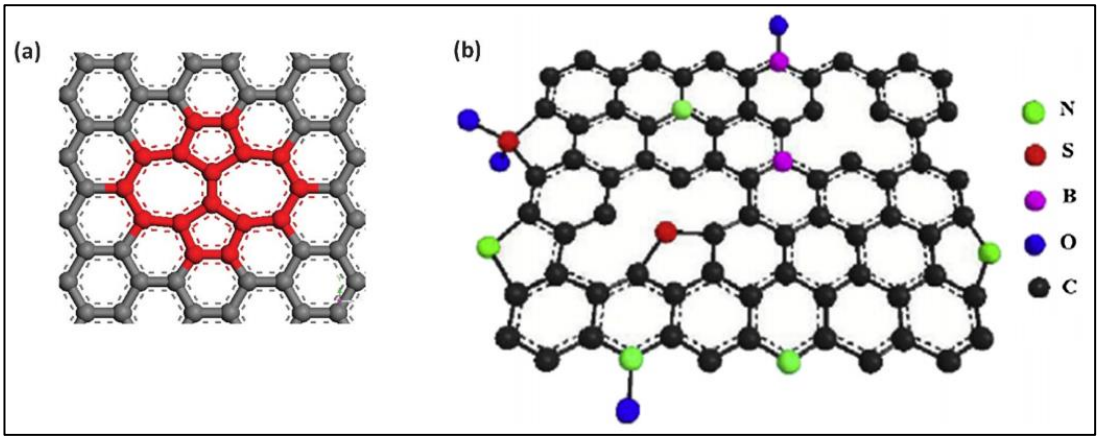

Figure 2.5 Graphene defects (a) intrinsic defect and (b) extrinsic defects [29]

Theoretically, graphene has a monolayer structure; nevertheless, the acceptance of graphene's structure has expanded to include multilayer configurations as well. These multilayers are composed of three distinct structures: AA, AB, and twisted layers, as shown in Figure 2.6. The AA stacked graphene is when each carbon atom is aligned with its counterpart carbon atom in the top and bottom layers. The AB stacking is considered more stable and known as the Bernal phase; it is bonded with only half of the upper carbon aligned with the lower carbon layer in the same manner as bulk graphite [30]. The structural spacing for both the AA and AB stacks, with the AB stack sharing nearly identical spacing (3.4 Å) with graphite [31]. This is why the AB stack inherits graphite's structural stability. In contrast, twisted layers occur when the graphene sheet layers are stacked with a slight twist of a few degrees (Figure 2.6). This slightly offset template, known as a Moiré pattern, generates AA and AB unit cells in the twisted lattice with an angle represented by θ [32].

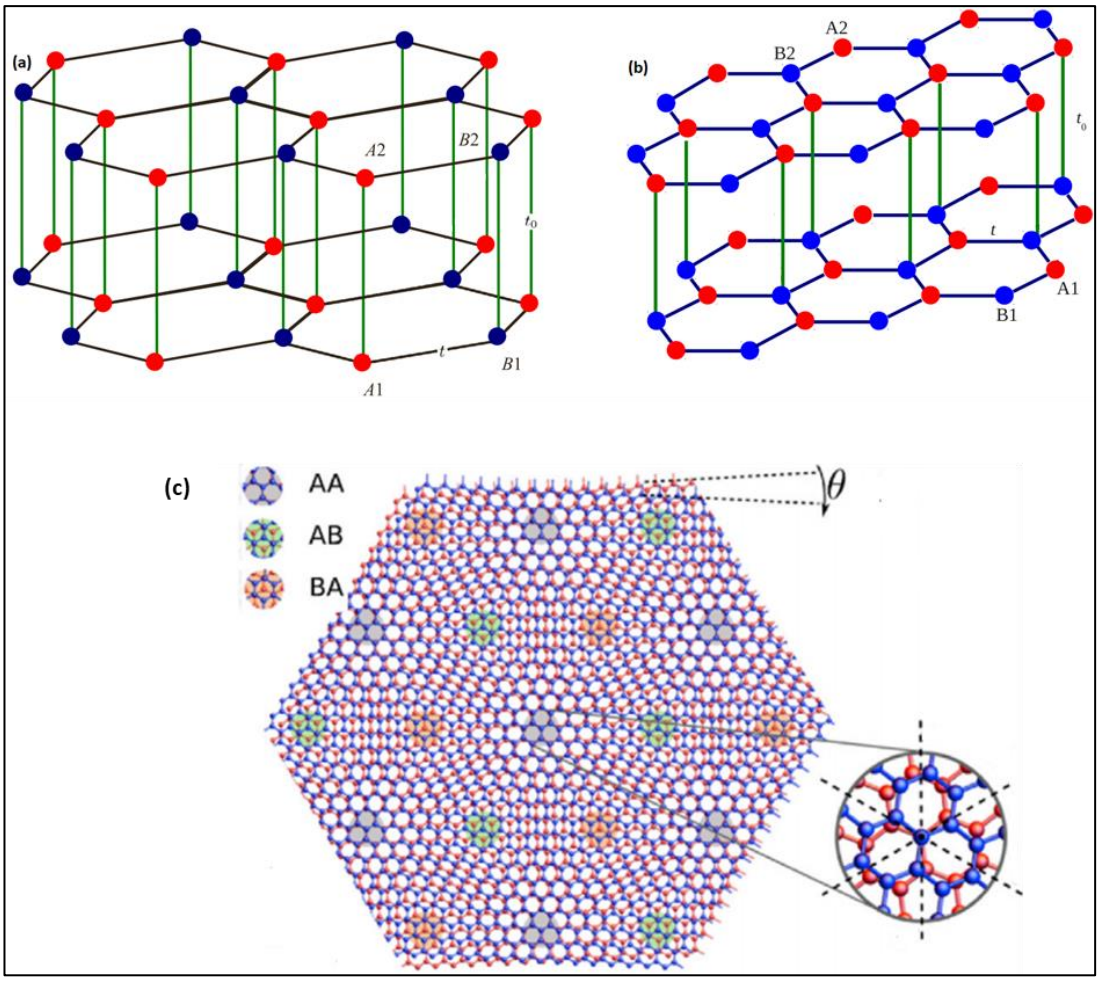

Figure 2.6 The illustration of multilayer structure for (a) AA stack, (b) AB stack, and (c) twisted layer with θ angle [32]

The capabilities of multilayer graphene are comparable to those of monolayer graphene. The electrical mobility, mechanical strength, durability, and flexibility of multilayer graphene are nearly equal to those of pristine graphene, which is why multilayers can be considered as graphene. Multilayer structures are advantageous due to their electrical and optical features, particularly their potential to widen the band gap [33]. This can be accomplished using techniques such as chemical doping and electrostatic activation, which disrupt the graphene's structural equilibrium. Figure 2.7 shows the band gap difference for mono- and multilayer as studied by Zhang et al. [30]. As stated, graphene with a single sheet, or pristine graphene in general, lacks a

band gap. Multiple layers of defective sites can be chemically doped to generate low-energy band formation, producing a cowboy hat-shaped energy gap. Dual-gate formation of multilayer graphene permits unorthodox tuning of the electrical field across the two layers, enhancing the total charge carrier density to a level appropriate for transistor devices.

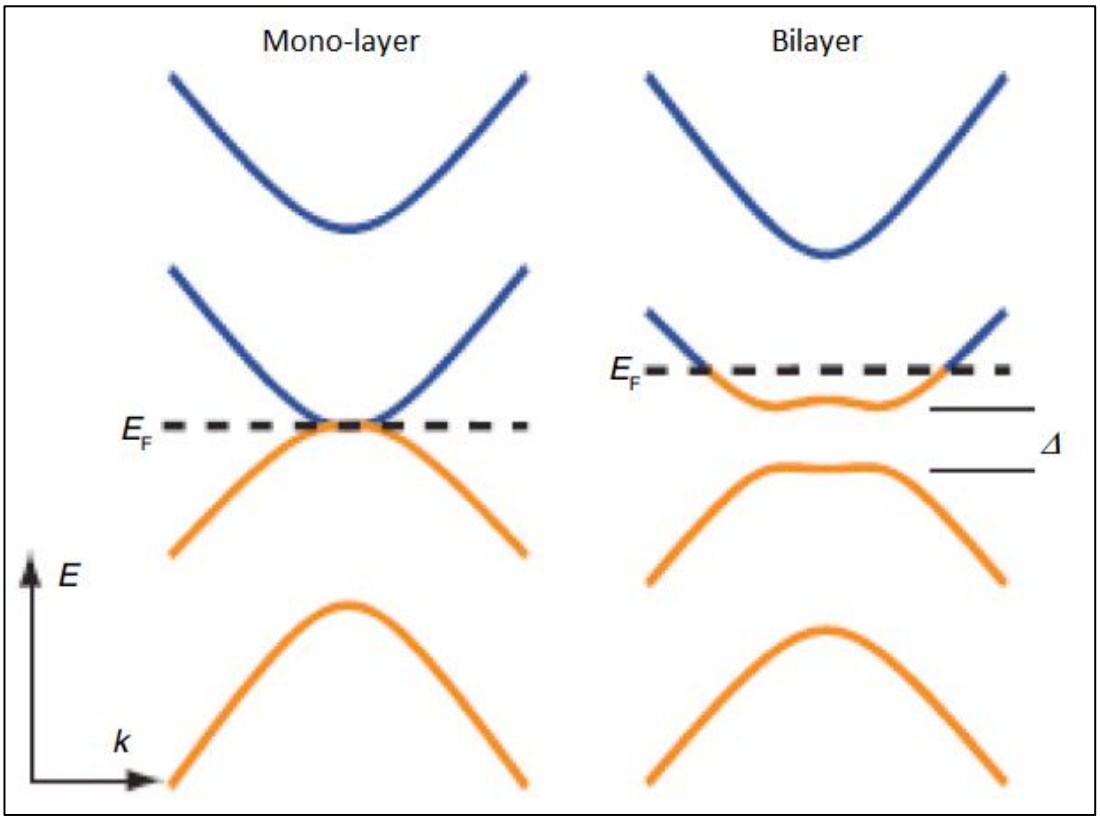

Figure 2.7 Band structure for pristine graphene and multilayer graphene [30]

Given that several studies have proved the adaptability of graphene's structure, industry interest in graphene as a nanomaterial structure has developed over the years. According to a market analysis conducted by IDTechEx, graphene's market will expand from $100 million in 2020 to $700 million by 2031 [7]. Schmaltz et al. reported that the current graphene's market is dominated by Asian players that claim nearly all top position as the major company that produces graphene [34]. China is the leading

country manipulating the graphene's market as China is abundant with widely distributed natural graphite mineralization zones and is the leading technology development of graphene, as reported by Pingkuo et al. [35]. Graphene's core market has been the multilayer graphene, and more companies are beginning to adopt graphene as their raw material, replacing other carbon-based materials.

2.1.2 Synthesis of Graphene and its Derivative

In recent years, various synthesis techniques have been established for graphene and its derivatives. The synthesis methods of graphene are a vital phase as they have an essential effect on the structure of graphene produced. Quality and purity are based on the pristine graphene structure, where more defects and impurities translate to lower quality and lower purity. However, defective graphene still has its market value because of its enabled doping ability that can improve its properties, especially in the field of electronics [36].

2.1.2(a) Mechanical Exfoliation

Mechanical exfoliation is a simple and repeatable method that is capable of giving multilayer graphene. Furthermore, graphene produced from this method is one of the highest quality multilayer graphene as evaluated with Raman, atomic force microscopy (AFM), and optical microscope with a bargain in the cost of production [37]. However, one drawback of using this method was its yield directly affecting its scalability [38]. Basically, the mechanical exfoliation method creates a sheer force on the graphite layers and overcomes the van der Waals attraction, which is exfoliated into graphene layers, as shown in Figure 2.8.

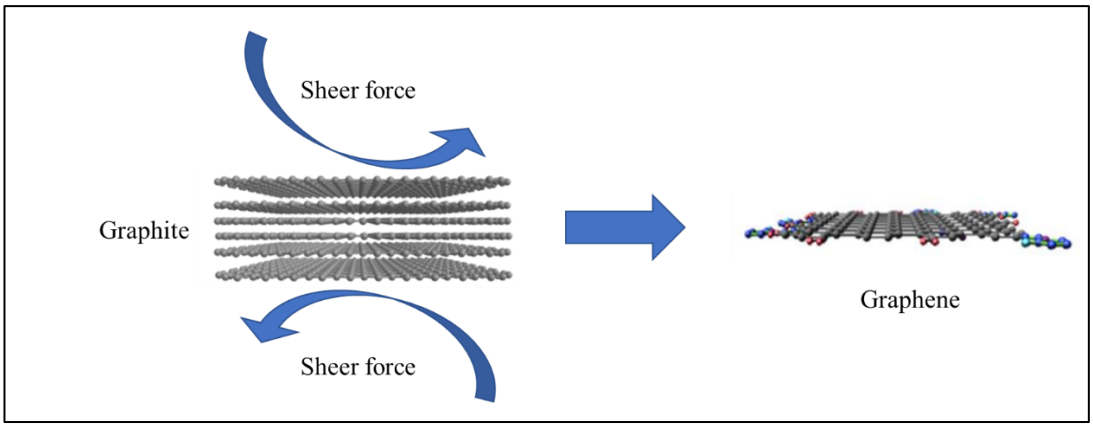

Figure 2.8 Mechanical routes using sheer force to separate graphene layers [38]

Minimizing the fragmentation effects is essential for producing a smaller size of graphene. The sonication method can create high-speed shock waves in the graphite structure, separating the graphene layers without fragmentation effects by controlling the power, medium, and centrifugation rate [39]. Zhang et al. prepared a few-layers graphene by utilizing a carbon sphere solution and graphite powder in a microfluidic homogenizer with a cyclic treatment under a certain pressure [40]. The collision between the carbon sphere and graphite powder produced 2-5 layers of graphene. Similarly, Joyner et al. utilized a mechanical exfoliation involving graphite powder suspended in a polyacrylonitrile electro-spinning instrument [41]. An electro-spinning instrument is a unit with a 26.7 mm (diameter) syringe where the graphite solution was transferred into the syringe before voltage and pressure were applied.

Meanwhile, Huang et al. introduced a process with two steps that enhanced and homogenized the adhesion force between the outermost sheets in contact with the multilayer graphite by submitting the substrate and controlling the level of forces between the loaded crystal layer(s) and the substrate [42]. The processes increased the yield and area of the graphene flakes produced more than 50 times compared to standard mechanical exfoliation methods. The ball milling technique also can be used

to exfoliate graphite mechanically. It features the sheer force technique and reduces the impacts between the sheets and the ball during the rolling actions, thus causing minor fragmentation effects.

2.1.2(b) Chemical Exfoliation

In principle, chemical exfoliation (liquid-phase exfoliation) gives a higher yield of graphene production than mechanical exfoliation. Generally, chemical exfoliation is a two steps method. The first step is to separate the interlayer of graphite by introducing a substance from a liquid chemical (electrolyte) between the layers, thus increasing the interlayer spacing. Then the graphite will exfoliate into graphene layers by heat or sonication [43]. Some chemical exfoliation methods are based on the chemical modification of graphite (e.g., graphite oxide), followed by separation [44]; others use small molecules to force in between the layers to create intermediate compounds known as graphene-intercalated compounds [45]. There is also a wet chemical exfoliation (electrochemical) method that can produce large quantities of graphene. A voltage was applied to drive the ion toward the graphite electrode to form gaseous molecules, intercalating and forcing the exfoliation process [46]. Upon continuing with the reaction, the graphite electrode will reduce in volume while graphene flakes can be seen deposited into the electrolyte, as shown in Figure 2.9. Combination with the sonication method can help to disrupt the graphite layers further.

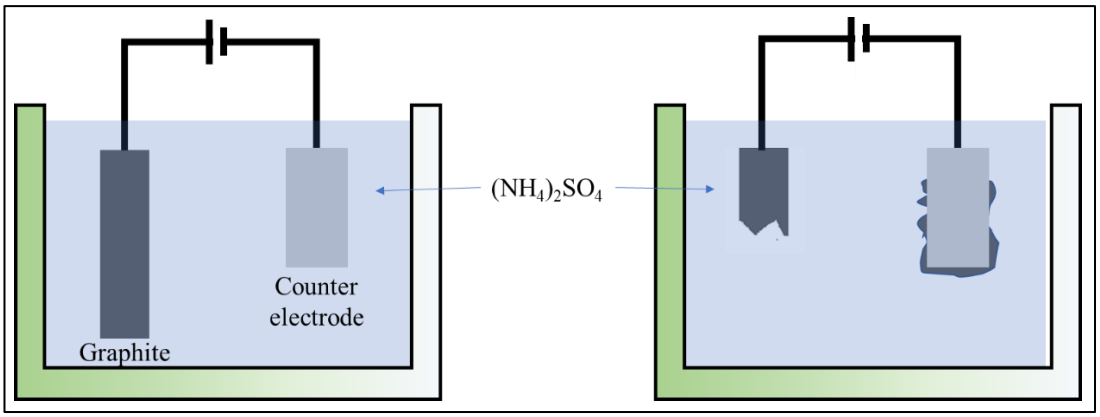

Figure 2.9 Electrochemical method of graphite used as electrode resulting in graphene flakes deposited into the electrolyte [47]

Table 2.1 shows the list of liquid exfoliation methods with the help of a sonicator. Although sonication can be categorized as mechanical exfoliation, the solvent's use helped expand the graphite layer's spacing before finishing it with the sonication technique in a liquid-phase exfoliation. The flake size of graphene is susceptible to the sonicator's frequency and the sonication system's power. By controlling these two factors, which affect the flake size distribution of the produced graphene [48]. Water as a liquid medium is the most practical choice as it is non-toxic and cheap. However, given the nature of graphite being hydrophobic, making dispersion onto the water is quite tricky. The use of surfactants has been recorded in many pieces of literature to enable better dispersion of graphite. Wang et al. studied the effect of surfactants in the water sonication of graphite [49]. Both ionic and non-ionic surfactants can be used to help in producing large sheets of graphene.

Table 2.1 List of chemical exfoliation methods with the help of the sonicator

Material	**Liquid medium**	**Details**	**Graphene**	**Ref**
Graphite fine powder	PVP + H_2O	Sonicator bath, 135 W, 9 h, centrifuge 1500 rpm.	Thickness of < 1 nm. Low D band. High G band.	[50]
Graphite powder	O_3 + H_2O	Sonicator bath, 80 W, 23 kHz, 15 h.	Multilayers. Thickness of 13 nm. Low D band. High G band.	[51]
Bulk graphite	H_2O	Sonicator bath, 20 kHz, 72 h.	Single, bi, multilayers. Thickness of < 100 nm. High D band. High G band.	[52]
Graphite powder	H_2O + SDS (surfactant)	Tip sonicator, 100 W, 12 h.	Single, multilayers. Thickness of 35 nm. Low D band. High G band.	[53]
Graphite flakes	Ethanol + H_2O	Tip sonicator, 300 W, 2 h.	Nanoplatelets. Thickness of 10 nm. Low D band. High G band.	[54]
Graphite powder	Silk nanofiber + H_2O	Tip sonicator, 195 W, 1 h, centrifuged 1500 rpm.	Few layers. Thickness of 2 nm. Low D band. High G band.	[55]

Graphite powder	H_2O + SDOC (surfactant)	Sonicator bath, 100 W, 8 h, centrifuged 1500 rpm.	Large size, few layers. Thickness of < 1 nm. Low D band. High G band.	[49]
Graphite powder	Acetone + H_2O	Sonicator bath, 0.8 W, 2 - 12 h, centrifuged 500 – 4000 rpm.	Defect-free. Thickness of < 1 nm. Low D band intensity. High G band intensity	[56]
Graphite powder	Pyrene + H_2O	Sonicator bath, 600 W, 420 h, centrifuged 3500 rpm.	Single, few layers. thickness of 50 nm. Low D band. High G band.	[57]

PVP = polyvinylpyrrolidone, O_3 = ozone, SDS, sodium dodecyl sulfate, SDOC = Sodium deoxycholate.

It should be noted that in the electrochemical process, there are possibilities that the intercalate process can start randomly on the graphite electrode, which is troublesome when the exfoliation process is concentrated in the middle of the electrode. This scenario heavily influences the efficiency as it will stop the reaction process on the disconnected electrode. Moreover, the usage of chemicals essentially removes any potential for green synthesis. Apart from that, separating the graphene flakes from the counter electrode will require an additional step, resulting in an increase in the overall cost.

2.1.2(c) Chemical Vapor Deposition

CVD is not considered an exfoliation method as the carbon source is not graphite but gaseous materials. The gaseous carbon will re-arrange itself from the ground up and form a graphene structure which is not similar to tearing the graphite layers. A transition metal was placed in contact with different gaseous hydrocarbon precursors at a high temperature within the reaction chamber. In terms of functionality, the graphene produced possesses a high surface area which is a promising material in many energy-related applications. However, the downside of this method is its high production cost, low output, transferability, and purification method, a step needed to remove the residue catalyst used during CVD [58]. Even with the downside of this method, its ability to produce a large quantity of pristine graphene makes it better than any other method. Depending on the carbon solubility, metals with low carbon solubility will form the nucleation sites on the metal catalyst surface and extend in all directions from these sites until it covers the metal surface [59] (Figure 2.10). However, metals with high carbon solubility will diffuse/dissolve the carbon precursor on the heated metal surface, bonded and segregated to the top, forming graphene sheets around the metal surface [60].

These two different carbon solubility metals affect the outcome of graphene produced. High carbon solubility will produce sizable graphene depending on the cooling temperature, while low carbon solubility will produce sizable graphene depending on the metal surface's size. In order to transfer the graphene from its metal surface, the graphene layers were detached by a chemical etching process on the metal substrate. Although it counts as an extra step in terms of efficiency, this method is considered easy and not too complicated in creating high-quality graphene layers.

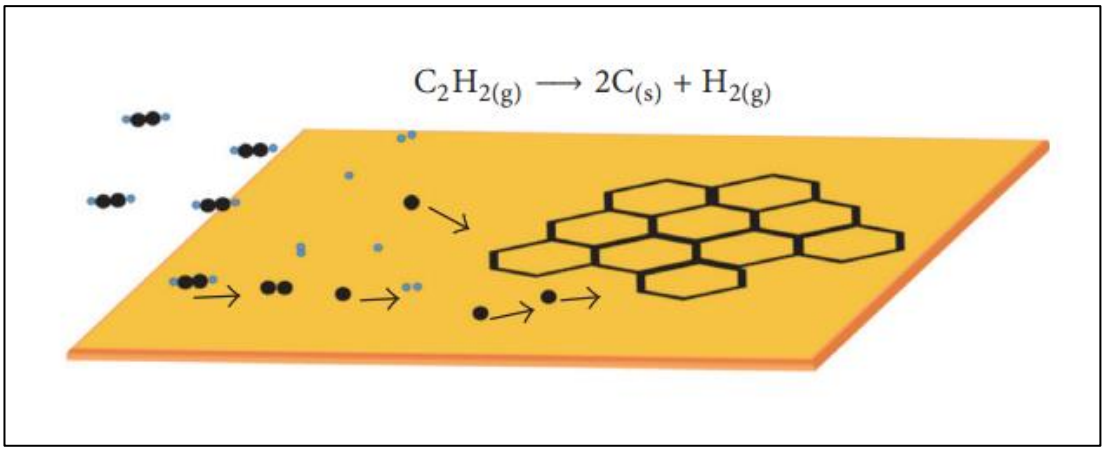

Figure 2.10 Schematic of the graphene CVD mechanism [61]

It should be noted that the process of high growth depends heavily on temperature and a long cooling process. Table 2.2 shows a list of CVD methods with rapid growth time and low defect graphene produced and noted that many of them used a temperature of around 1000 °C. The high temperature will affect the overall process and efficiency as higher temperature requires more energy and a longer cooling process. Tu et al. found that the optimal cooling rate is a shorter cooling time of around 10 °C/s. If the rate is more than that, it will result in the formation of graphene with more defects [62].

Table 2.2 Graphene CVD recipes on primary metal substrates

CVD Method	Growth substrates	Carbon Source	Growth conditions	Graphene morphology	Ref.
LT-CVD	Cu	CH_4	Temp: 400 °C Atm: Ar, H_2 Gas flow: 10 / 10 sccm	Low-porous, nanowall graphene. ($I_D/I_G < 0.9$)	[63]
RT-CVD	Ni	CH_4	Temp: 1000 °C Atm: H_2, N_2 Gas flow: 100 / 700 sccm Growth time: 10 s	Large area, graphene film with high optical transmittance ($I_{2D}/I_G = 1.15$)	[64]
RT-CVD	Cu	CH_4	Temp: 970 °C Atm: N_2, Gas flow: 5000 sccm Growth time: 15 min	Large area (400 × 300 mm^2) graphene. ($I_{2D}/I_G = 0.9$)	[65]
UHV-CVD	Pt (111)	C_2H_4	Temp: ~700 °C Atm: Ar Growth time: 250 s	Monolayer, island (> 10μm diameter) graphene	[66]
T-CVD	Cu	CH_4	Temp: 1050 °C Atm: H_2 Gas flow: 500 sccm	Large area, monolayer graphene. ($I_D/I_G < 0.05$)	[67]